



Published in final edited form as:

ACS Chem Biol. 2014 January 17; 9(1): 227–236. doi:10.1021/cb400581f.

Direct Observation of Multiple Tautomers of Oxythiamine and their Recognition by the Thiamine Pyrophosphate Riboswitch

Vipender Singh^{†,‡,¶}, Chunte Sam Peng[†], Deyu Li^{†,‡,¶}, Koyel Mitra[§], Katherine J. Silvestre[¶], Andrei Tokmakoff^{†,¶}, and John M. Essigmann^{†,‡,¶,*}

[†]Department of Chemistry, Massachusetts Institute of Technology, Cambridge, MA 02139

[‡]Department of Biological Engineering, Massachusetts Institute of Technology, Cambridge, MA 02139

[¶]Center for Environmental Health Sciences, Massachusetts Institute of Technology Cambridge, MA 02139

Abstract

Structural diversification of canonical nucleic acid bases and nucleotide analogues by tautomerism has been proposed to be a powerful on/off switching mechanism allowing regulation of many biological processes mediated by RNA enzymes and aptamers. Despite the suspected biological importance of tautomerism, attempts to observe minor tautomeric forms in nucleic acid or hybrid nucleic acid-ligand complexes have met with challenges due to the lack of sensitive methods. Here, a combination of spectroscopic, biochemical and computational tools probed tautomerism in the context of an RNA aptamer-ligand complex; studies involved a model ligand, oxythiamine pyrophosphate (OxyTPP), bound to the thiamine pyrophosphate (TPP) riboswitch (an RNA aptamer) as well as its unbound non-phosphorylated form, oxythiamine (OxyT). OxyTPP, like canonical heteroaromatic nucleic acid bases, has a pyrimidine ring that forms hydrogen bonding interactions with the riboswitch. Tautomerism was established using two-dimensional infrared (2D IR) spectroscopy, variable temperature FTIR and NMR spectroscopies, binding isotope effects (BIEs) and computational methods. All three possible tautomers of OxyT, including the minor enol tautomer, were directly identified and their distributions were quantitated. In the bound form, BIE data suggested that OxyTPP existed as a 4'-keto tautomer that was likely protonated at the N1'-position. These results also provide a mechanistic framework for understanding the activation of riboswitch in response to deamination of the active form of vitamin B1 (or TPP). The combination of methods reported here revealing the fine details of tautomerism can be applied to other systems where the importance of tautomerism is suspected.

The heterocyclic bases of RNA and DNA can exist in optional tautomeric states, which has significant implications for nucleic acid biochemistry.(1–13) In RNA, formation of optional tautomeric forms is speculated to play a role in catalysis and binding by RNA enzymes and aptamers.(1–5, 14) Small self-cleaving RNA enzymes such as Hammerhead, Varkud Satellite, Hairpin and *GlmS* have been proposed to utilize either the ionized forms or the minor enol or imino tautomeric forms or both of conserved guanines, in which the N1

*To whom correspondence should be addressed: Mailing Address: Room 56-669; 77 Massachusetts Avenue, Cambridge, MA 02139
Telephone number: 617-253-6227. jessig@mit.edu.

[¶]Present address: University of Chicago, 929 E. 57th St., Chicago, IL 60637.

[§]Current Address: Dept. of Medicine, University of California San Diego, 9500 Gilman Drive, San Diego, CA 92122

The authors declare no competing financial interest.

Supporting Information

This material is available free of charge via the Internet at <http://pubs.acs.org/>.

position is deprotonated, to perform their catalytic functions.(2–4, 15–19) Tautomeric preference has also been proposed in the recognition of ligands and inhibitors by certain RNA aptamers, the purine and the thiamine pyrophosphate (TPP) riboswitches. The purine riboswitch, which regulates genes involved in guanine metabolism, has been suggested to bind to the enol tautomer of xanthine(1) whereas the TPP riboswitch has been proposed to recognize oxythiamine pyrophosphate (OxyTPP), a model) ligand, in its enol form instead of the more standard keto tautomer.(14 The importance of tautomerism has also been proposed in DNA replication where the occurrence of minor tautomeric forms during replication could lead to mutations.(6–12, 20) Indeed Watson and Crick suggested that correct base pairing in DNA requires nucleic acid bases occurring in their predominant tautomeric states.(21, 22) There is a growing appreciation of the significant potential biological implications of tautomer formation in nucleic acid biochemistry.(13)

Despite the biological importance of tautomerism, it has been challenging to observe minor tautomeric forms owing to the lack of sensitive methods. For example, using x-ray crystallography, at typical resolutions, it is often difficult to unambiguously assign the position of protons to distinguish various tautomeric forms.(1, 14, 23) Tautomerism is also difficult to study using electronic spectroscopy because the spectra associated with multiple tautomers are usually broad and featureless.(24–26) NMR spectroscopy, although sensitive to tautomerization, is challenging for observing tautomers in aqueous solution at room temperature because under these conditions the exchange rates between tautomers can be faster than the NMR time scale.(27) Vibrational spectroscopy, such as FTIR and Raman, have been used for studying tautomerism under non-physiological gas phase conditions; however, these conditions do not replicate tautomeric distribution present under biologically relevant aqueous conditions.(28–30) In the gas phase, tautomer distribution often favors minor tautomers, even for canonical nucleic acid base pairs.(28, 30) Systematic studies of tautomerism are not only lacking in the context of nucleic acid or nucleic acid-ligand complexes, but there is also little direct evidence to demonstrate that such isomerizations occur within the context of these complex systems. Although, the chemical features such as ionized states or altered pK_a of nucleic acid bases in ribozymes have been extensively studied,(17–19, 31–34) a survey of the literature suggests that progress in studying tautomerism is limited by the lack of suitable methods to detect tautomeric species under aqueous conditions.

The present study undertook the application of solution-based methods to reveal the presence of minor tautomeric forms in molecules, overcoming the obstacles of their fast interconversion rates, very similar chemical properties and complexity of the nucleic acids systems. In this study, the tautomeric form of OxyTPP (Figure 1A) was characterized in the context of TPP riboswitch (Figure 1B) using methods based on binding isotope effects (BIEs) and density functional theory (DFT) calculations. BIEs, which report on changes in the vibrational properties of a bond between the bound and unbound states, together with DFT calculations allowed us to determine the tautomeric form of OxyTPP bound to the TPP riboswitch. We also determined all possible tautomers of the unbound non-phosphorylated form of its ligand, OxyT (Figure 1A), including its minor tautomeric forms using variable temperature conditions. 2D IR spectroscopy is an emerging new method to characterize tautomeric equilibria under aqueous conditions.(35) It has a picosecond time resolution, which allows direct observation of the tautomerization process using a fast triggering method such as temperature-jump.(36) In the present work, the combination of methods based on 2D IR, FTIR, variable temperature NMR, BIEs and DFT calculations allowed us to fully characterize tautomeric forms of the ligand in-solution and bound to the TPP riboswitch under biologically relevant aqueous equilibrium conditions. We also provide an estimate of the exchange rates for interconversion of tautomers via performing low temperature NMR experiments.

Results and Discussion

The thiamine pyrophosphate riboswitch bound to OxyTPP (Figure 1B) provides a good model system for comprehensively studying tautomerism in nucleic acid complexes because structural studies have predicted that the riboswitch binds to the minor tautomeric form of OxyTPP. OxyTPP, like the nucleic acid bases, has a heteroaromatic ring system that forms hydrogen bonding interactions with the riboswitch (14) and, in the unbound form the OxyT part of OxyTPP can theoretically exist in three tautomeric forms depending on the position of the active proton (Figure 2): two 4'-keto forms that are protonated either at the N1'-position (4'-keto-N1'H-OxyT) or at the N3'-position (4'-keto-N3'H-OxyT) and a 4'-enol (4'-enol-OxyT) form. Below we determine the tautomeric forms of OxyT in the absence of RNA and its diphosphorylated form, OxyTPP, bound to the TPP riboswitch.

Tautomers of OxyT in the unbound form

Traditional NMR approaches could not resolve tautomeric forms of OxyT under physiological aqueous conditions because tautomerization of this type of heterocycle occurs on nanosecond time scales (36) (Supplementary material; Note 1); therefore, 2D IR spectroscopy, an optical analogue of 2D NMR with picosecond time resolution, was used to characterize all possible tautomeric forms of OxyT.

Experimentally, tautomerism of OxyT was investigated by variable temperature FTIR and 2D IR experiments in TPP buffer (1M HEPES buffer pH 7.5, 100 mM KCl and 15 mM MgCl₂; Supplementary Table S1). The variable temperature FTIR spectra of OxyT in the region of in-plane double bond vibrations for aromatic heterocycles are shown in Figure 3A. Vibrational bands in this region, which we number from high to low frequency, are expected to have a distinct pattern for each tautomer, in particular when the C=O character is altered significantly.(9, 35, 37) The X1 mode is composed of X1a at 1658 cm⁻¹ with a shoulder (X1b) at 1646 cm⁻¹. The X1 mode was assigned to the carbonyl stretch in the keto form of OxyT based on the characteristic vibrational frequency, high IR intensity, and the broad line-shape.

The 2D IR spectrum of OxyT in TPP buffer at 10 °C is shown in Figure 3B. Analogous to 2D NMR, sequences of ultrafast IR pulses are employed in 2D IR experiments to excite molecular vibrations and detect energy flow to other vibrations. Each peak in a 2D IR spectrum contains a doublet with a positive feature (red) originating from the ground state absorption and stimulated emission, and a negative contribution (blue) due to the excited state absorption. A typical 2D IR spectrum consists of diagonal peaks that correspond to the FTIR peaks, and off-diagonal cross-peaks, if the vibrations are coupled. As a consequence, the correlation of excitation (ω_1) and detection (ω_3) frequencies in a 2D IR spectrum allows mixtures of chemical species such as structural isomers or tautomers to be resolved through the cross-peaks that encode their intramolecular vibrational couplings.(35, 38, 39) The 2D IR study on nucleic acid bases in the fingerprint region has shown that intense cross-peaks exist between all of the diagonal peaks due to the delocalized nature of these carbonyl and ring vibrations in the aromatic system.(40) Therefore, the contrast between the pronounced X1a/X4 cross-peaks at (ω_1, ω_3) = (1658 cm⁻¹, 1525 cm⁻¹) and the absence of X1b/X4 cross-peaks clearly indicate that X1a and X1b originate from two different species.

The DFT frequency calculations predicted that the C=O frequency of the 4'-keto-N3'H-OxyT tautomer is slightly lower than that of the 4'-keto-N1'H-OxyT, suggesting that the X1b shoulder is from the C=O stretch of the 4'-keto-N3'H-OxyT (Figure 3C and Supplementary Figure S1 and S2). The calculations also show that both keto tautomers have a peak at ~ 1545 cm⁻¹ corresponding to the pyrimidine ring vibrations with strong C=N character. This peak matches well with the experimental peak at 1558 cm⁻¹ (X3), which has cross-peaks to

both C=O peaks. Furthermore, the calculations showed that the 4'-keto-N1'H-OxyT tautomer has noticeable methyl group vibrations that contribute to the 1450 cm⁻¹ band, whereas the 4'-keto-N3'H-OxyT tautomer has a much weaker peak at 1450 cm⁻¹. The intensity difference in the methyl vibration manifested itself in the 2D IR spectrum where cross-peaks were observed between X1a/X4 but not between X1b/X4. Finally, an unusually broad peak (X2) was seen at 1598 cm⁻¹, which also has cross-peaks to X4. Again comparing it to the DFT calculations, X2 was assigned to be the collective ring vibration of the enol tautomer that involves the C=N stretches as well as the O-D stretch coupled to the water vibrations (Supplementary Figure S3). The 4'-enol-OxyT tautomer had an even more intense methyl vibration than the 4'-keto-N1'H-OxyT tautomer, which resulted in the cross-peaks between X2/X4. The distinct cross-peak patterns in the 2D IR spectrum enabled us to identify and distinguish among all three tautomers of OxyT under relatively physiological conditions.

Since the three tautomers have distinct peaks at 1658 cm⁻¹, 1646 cm⁻¹, and 1598 cm⁻¹ for the 4'-keto-N1'H-OxyT, 4'-keto-N3'H-OxyT, and 4'-enol-OxyT, respectively, their relative populations can be extracted out by simultaneously fitting the FTIR and 2D IR spectra in the 1580 – 1700 cm⁻¹ frequency range (Supplementary Method M1).^(37, 41) A self-consistent fitting of the FTIR and 2D IR spectra at room temperature resulted in 8% ± 1% 4'-enol-OxyT tautomer, 55% ± 5% 4'-keto-N1'H-OxyT and 37% ± 7% 4'-keto-N3'H-OxyT tautomers (Figure 3D and Supplementary Table S2). The variable temperature FTIR spectra show that X1a intensifies at the expense of the X1b shoulder as the temperature is raised, whereas X2 has weak temperature dependence. Fitting the variable temperature FT IR spectra using the spectroscopic parameters from the room temperature spectra showed that the 4'-keto-N1'H-OxyT population increased to ~ 70% at 90 °C, the 4'-keto-N3'H-OxyT population decreased to ~ 20%, whereas the 4'-enol-OxyT tautomer was relatively constant within the error bars (Figure 3D and Supplementary Figure S5).

As indicated above, the IR methods allowed us to observe all possible tautomeric forms of OxyT under physiologically relevant aqueous conditions. The presence of different tautomeric forms of OxyT was also established by 1D and 2D and variable-temperature NMR experiments. NMR experiments were performed in DMF to prevent fast exchange of the active proton on the ligand and water, and at low temperature such that the tautomeric interconversion rate is slow enough to resolve all three tautomers. Initially, by correlating the data generated from 2D NMR techniques such as COSY, HSQC, and HMBC, all non-active proton and carbon signals were assigned to the corresponding positions on OxyT (Supplementary Table S3). The active proton on the pyrimidine ring of OxyT, which is expected to have different chemical shifts in various tautomers of OxyT, was studied by the NMR spectra in DMF from 20 °C to -60 °C (Figure 4A). At -60 °C three distinct proton resonances between 12.5 to 17.0ppm were observed that were attributable to protons bound either to N1' or N3' or to the 4'-oxygen on the pyrimidine ring. Considering that each tautomer can only have the proton at one of these three positions, the presence of three proton resonances indicated the presence of three tautomeric forms of OxyT in DMF solvent at -60 °C.

Based upon a comparison to the literature, the proton resonance at 16.6ppm was assigned to the N3' amide proton in the 4'-keto-N3'H-OxyT tautomer (Figure 4A), 15.5ppm to the 4'-enol-OxyT proton, and 13.3ppm to the N1' amino proton in the 4'-keto-N1'H-OxyT tautomer (Supplementary material; Note 1). Integration and normalization of these peaks permitted determination of the relative ratios of the three tautomeric species that exist in DMF at low temperature (4'-keto-N3'H-OxyT: 4'-enol-OxyT: 4'-keto-N1'H-OxyT = 0.34 : 0.38 : 0.28). The difference in the ratios between 2D IR and NMR was attributed more to the solvent conditions than to temperature, since H₂O is required for the tautomer exchange process. The separation of chemical shifts for three tautomers also allowed us to estimate the

timescale of exchange among tautomers, which was between 0.27 to 0.82 milliseconds at $-50\text{ }^{\circ}\text{C}$, which is the coalescence temperature for the exchange among different tautomers (Supplementary material; Note 2). In contrast to OxyT, variable temperature NMR data for thiamine indicated that it was present in solution as a single 4'-amino tautomer (Figure 4B).

Tautomeric form of OxyTPP bound to the TPP riboswitch

The spectroscopic approaches described above allowed us to characterize the tautomeric forms of OxyT in the unbound form. Given the complexity of the TPP aptamer, these approaches could not be directly applied to determine the tautomeric form of OxyTPP bound to the riboswitch. To establish the tautomeric form of the bound OxyTPP we used experimental binding isotope effects (BIEs), which characterize the increase or decrease in binding upon substitution of an atom with its heavier isotope.⁽⁴²⁾ BIEs are useful as they are sensitive to change in bond order between two equilibrium states and are influenced by alterations in vibrational frequencies between the bound and the unbound states of a ligand, such as those described for the tautomers above. In general, if a bond order to an atom with the substitution decreases upon binding, it is the lighter isotope that binds better and a BIE of greater than 1.0 is observed. An inverse BIE or a BIE of less than 1.0 is indicative of an increase in bond order upon binding or tighter binding of the heavier isotope. The magnitude of the effect is correlated with the change in bond order. BIEs have been used to study enzyme-substrate interactions in enzymes such as dehydrogenases and to detect subtle changes in bonding in glucose when bound to the hexokinase enzyme.^(43–46)

The ^{18}O BIE at the 4'-position of OxyTPP, $4'\text{-}^{18}\text{O}$ BIE, along with DFT calculations were used to establish the tautomeric form of OxyTPP bound to the TPP riboswitch. Given the small magnitude of ^{18}O isotope effects, to achieve the necessary precision BIEs were measured in the competitive condition. The light and heavy ligands were mixed in the same reaction and the ratios were quantitated for the bound and the unbound forms. To distinguish OxyTPPs labeled with the light ^{16}O and the heavy ^{18}O oxygen isotopes, they were double labeled with ^{32}P and ^{33}P radioisotopes, respectively, at the terminal pyrophosphate position and were quantitated by scintillation counting. An isotope effect of 0.987 ± 0.002 (mean \pm std. error) was measured for OxyTPP that was double labeled with ^{18}O and ^{33}P and ^{16}O and ^{32}P at the 4'-oxygen and terminal phosphate positions. BIE values were corrected for an ^{18}O enrichment factor of 0.725 measured using quadrupole time-of-flight (QTOF) mass spectrometry for the synthesized OxyT (Supplementary Figure S6). The BIE measured using ^{18}O and ^{33}P double labeled OxyTPP was also corrected for a small BIE of 1.004 ± 0.0035 for the ^{33}P substitution, measured in a separate experiment using ^{33}P and ^{32}P labeled OxyTPP molecules. The final $4'\text{-}^{18}\text{O}$ BIE of 0.982 ± 0.004 was obtained after the correction (Figure 5). A systematic isotope effect of close to unity (1.001 ± 0.002) was obtained from the experiment in the absence of riboswitch. The double labeling procedure also allowed the flexibility of measuring the $4'\text{-}^{18}\text{O}$ BIE by switching the labels of OxyTPP, by combining ^{18}O with ^{32}P and ^{16}O with ^{33}P . The BIE of 0.985 ± 0.004 was measured using these labeling combinations, within the error of the value obtained with the opposite pairing (Figure 5). The approximate average of the two $4'\text{-}^{18}\text{O}$ BIE values, from opposite pairings, of 0.984 was used in subsequent analysis. The experiment was repeated multiple times; the inverse values were obtained only when the ^{18}O isotope were incorporated into the labeling scheme. A titration experiment using TPP further confirmed that the small inverse O-18 BIE comes from specific binding of OxyTPP to the binding pocket of the TPP riboswitch (Supplementary Table S4). Errors were propagated using the product rule.⁽⁴⁷⁾

The inverse $4'\text{-}^{18}\text{O}$ BIE value of 0.984 suggested that the binding of OxyTPP to the TPP riboswitch resulted in increased bonding to the 4'-oxygen of OxyTPP, which is inconsistent with the presence of an enol tautomer in the bound form in its neutral form. The 4'-carbonyl group of the OxyTPP has a double bond character in the keto isomeric form compared to a

single bond in the enol isomer. However, in the enol form reduction in bond order to the 4'-carbonyl oxygen is partially compensated by formation of an additional bond to a hydrogen atom, which contributes inversely to the measured ^{18}O isotope effects. In order to dissect the relative contributions of these two effects, we analyzed the 4'- ^{18}O BIE computationally.

The expected magnitude of the 4'- ^{18}O BIE for the conversion of 4'-keto tautomer to 4'-enol tautomer was estimated using 4'-keto-N1'H-OxyT, the dominant unbound form and 4'-enol-OxyT. Although, OxyT can exist in three tautomeric forms, as shown above, the spectroscopic and thermodynamic analyses show that the 4'-keto-N1'H-OxyT form is lower in energy and more populated compared to the enol form (Figures 2 and 3D). A small normal 4'- ^{18}O BIE of 1.001 was calculated for the conversion of 4'-keto to 4'-enol tautomer (Supplementary Table S4), suggesting only a small decrease in bond order to the 4'-oxygen. The calculated BIE value however was significantly different than the experimentally observed value. The inverse BIE of 0.984 is indicative of increased bond order to the 4'-oxygen upon binding to the riboswitch. An inverse 4'- ^{18}O BIE is inconsistent not only with the existence of enol tautomer in the bound form but also with the observation that the 4'-enol group is hydrogen bonded to the neighboring guanine. Polarization of the 4'-enol group of OxyT due to hydrogen bonding would further increase the magnitude of normal 4'- ^{18}O BIE (Table 1).

The NMR data show that tautomers of OxyT interconvert on less than a millisecond time scale; it is therefore anticipated that any isotope effect arising from the conversion of one tautomer into another would contribute to the observed isotope effect. Binding of OxyTPP to the TPP riboswitch also involves a desolvation step and any isotope effect arising from this step would also be a part of the measured BIE. Calculations suggest that these factors contribute minimally to the observed BIE and do not account for the experimentally measured inverse BIE (Table 2 and Supplementary Table S5).

The inverse 4'- ^{18}O BIE, which is indicative of increase in bond order to the 4'-oxygen, can potentially arise from additional bonding, possibly a hydrogen bond with a functional group in the binding pocket of the TPP riboswitch. The Badger rule,(43) which relates the change in bond length with the alteration in stretching frequencies, suggests that hydrogen bonding to the 4'-oxygen of OxyTPP would contribute inversely to the observed 4'- ^{18}O BIE. This effect was mimicked by the bringing in of a water molecule close to the 4'-oxygen of OxyTPP. Formation of the hydrogen bond reduces the 4'- ^{18}O BIE and a full correlation between the calculated and experimental BIEs is observed at distances where a strong hydrogen bonding is predicted (Table 3).

The crystal structure of the TPP riboswitch with its ligand predicts that the pyrimidine ring of TPP forms two hydrogen bonds with G28, between the exocyclic 4'- NH_2 group of TPP and N3 of G28 and N3 of TPP and 2- NH_2 of G28 (Supplementary Figure S7).(48) The TPP-responsive riboswitch from *Arabidopsis thaliana* displays an apparent dissociation constant of ~ 50 nM for its natural ligand TPP,(48–50) with the binding of TPP to the riboswitch dependent on the concentration of Mg^{2+} ions.(51–53) The 4'-OxyTPP in the keto form is expected to bind unfavorably compared to TPP due to the potential loss of hydrogen bonding with N3 of G28. In addition, OxyTPP binding relative to TPP is expected to be entropically unfavorable as, in the unbound form, OxyT is present in multiple tautomeric forms compared to single tautomeric form for thiamine, as predicted above from the NMR experiments. Consistent with this observation OxyTPP, our model compound and presumably a natural metabolite of TPP, specifically binds to the TPP riboswitch with a K_d of $1.67 \mu\text{M}$ (Figure 6 and Supplementary Figure S8), an approximately 33-fold increase in dissociation constant over the natural ligand. Furthermore, in order to retain the hydrogen bond between the OxyTPP and G28 of the TPP riboswitch, the N3' atom of OxyTPP needs

to be in an unprotonated form, suggesting that the proton is present on the N1' atom, consistent with its crystal structure with the TPP riboswitch. It is therefore argued that the keto tautomer of OxyTPP that is protonated at the N1' position, 4'-keto-N1'H-OxyTPP, is the bound form of OxyTPP.

Taken together, the spectroscopic data show that 4'-keto-N1'H-OxyT is the predominant tautomeric state in the unbound form followed by 4'-keto-N3'H-OxyT and then 4'-enol-OxyT. In the bound form, the BIE data are consistent with the presence of 4'-keto-OxyTPP tautomer, which is also the predominant tautomer in the unbound state. Considering OxyT tautomers interconvert on the sub millisecond time scale, it is likely that the TPP riboswitch directly binds the 4'-keto-N1'H-OxyTPP tautomer and other tautomeric forms convert to 4'-keto-N1'H-OxyTPP in solution to restore the equilibrium distribution. Tautomerization is less likely to happen in the binding pocket, as it would require significant repositioning of functional groups and close matching of their pK_a values to facilitate proton transfer; however our data do not rule out that possibility.

The higher K_d for OxyTPP compared to TPP also provides a mechanistic framework for the riboswitch activation in response to natural deamination of TPP. Cellular biomolecules including nucleic acid bases undergo deamination-mediated damage constantly by variety of cellular processes to cause formation of oxidized products such as xanthine from guanine, hypoxanthine from adenine and uracil from cytosine.(54) Formation of these deaminated molecules is not only mutagenic to cells, but also results in the reduction of cellular concentrations of the undamaged biomolecules. Deamination of thiamine pyrophosphate (TPP) produces OxyTPP. The cellular concentration TPP is tightly regulated at low nanomolar levels.(55) The *Arabidopsis thaliana* TPP riboswitch, which is negatively regulated in response to TPP concentration, has a K_d of about 50 nM for TPP. Therefore, even a small decrease in TPP concentration would lead to activation of the riboswitch to restore the undamaged form of the biomolecule. Having a higher K_d for OxyTPP therefore provides a mechanistic advantage, as even a small deamination of TPP would reduce the concentration below its K_d to generate an unbound active form of the riboswitch.

Proposed model for binding of OxyTPP to the TPP riboswitch

Crystal structures of the TPP riboswitch in complex with various ligands reveal that guanine at the 28 position (G28) is critical for determining ligand specificity.(14, 48, 56) The X-ray structure of the riboswitch with the TPP ligand shows that the amino group at the 4'-position of TPP acts as a hydrogen bond donor to the N3 atom of G28.(48, 56) Structural studies of OxyTPP with the riboswitch shows that its hydrogen bonding interactions to G28 are almost identical to those of TPP.(14) OxyTPP has a carbonyl group at the 4'-position. Therefore, similar hydrogen bonding interactions for OxyTPP and G28 can be achieved by having either the OxyTPP in its enol form with a neutral G28 (Figure 7A) or the OxyTPP in its keto form and the N3 of the G28 is in the protonated form as shown in figure 7B. The BIE data predicted that OxyTPP was present in its keto tautomeric form, suggesting that it is likely that the N3 of G28 was protonated to form a hydrogen bond with the 4'-carbonyl oxygen of OxyTPP, as shown in figure 7B. Hydrogen bonding to OxyTPP is also consistent with the inverse BIE measured experimentally. Presence of altered guanine charge states or minor tautomeric forms has also been predicted in other RNA systems such as small self-cleaving ribozyme and riboswitches such as Hammerhead, Varkud Satellite, Hairpin and *GlmS* ribozymes.(1–5)

Conclusions and Perspective

This work utilized complementary tools to address the question of tautomerism in the context of a biologically important nucleic acid aptamer. It identifies each of the tautomers,

including the minor enol tautomer, of a model ligand in the unbound and the bound forms. The study also provides a biochemical basis of OxyTPP recognition by the TPP riboswitch and gives a glimpse of the mechanism by which activation of the riboswitch might occur in response to oxidative damage to vitamin B1. Spectroscopic methods based on 2D IR and variable temperature NMR along with BIE based approaches described here can be applied more generally to allow characterization of the tautomeric forms of ligands or substrates in other proteins and nucleic acid systems. Understanding tautomerism of the nucleic acid bases within these nucleic acid systems will aid our understanding of the importance of these processes in the regulation of riboswitches, RNA catalysis and in the areas of nucleic acid biochemistry where preference for a specific tautomer is proposed. These methods would also be directly applicable in understanding tautomeric preferences of DNA and RNA polymerases and their role in causing spontaneous mutations during DNA replication. Recently, it has been shown that tautomeric pyrimidine analogues can accelerate the mutation rate of RNA viruses to the extent that those viruses go extinct within a defined biological system.(57) The methods described here could also find direct application to support rational design of similar antiviral agents (Supplementary Figure S9).(57, 58)

Methods

NMR Analysis of OxyT

1D, 2D, and variable temperature NMR experiments were performed on Varian 500 MHz NMR spectrometers. The NMR sample is prepared by dissolving 10 mg OxyT in 1.0 ml DMF-d₇. The ¹H NMR spectra are reported in parts per million (ppm) and were referenced to the signals for DMF-d₇ (2.73 ppm). The ¹³C NMR spectra were referenced to the signals for DMF-d₇ (30.1ppm).

Infrared Spectroscopy of OxyT

For both FTIR and 2D IR measurements, the H/D exchanged oxythiamine was dissolved at a concentration of 20 mg/ml in a buffer containing 1.0 M HEPES, 100 mM KCl and 15 mM MgCl₂ in D₂O. The high concentration of HEPES was required in the IR experiments to maintain the pH near neutral for the high concentration of OxyT. About 25 μ l of sample solution was sandwiched between two CaF₂ windows that are separated by a 50 μ m Teflon spacer. Variable-temperature FTIR spectra were collected using Nicolet 380 FT IR spectrometer at 1.0 cm⁻¹ resolution with 16 scans per spectrum. Spectra were acquired from 5.2 °C to 91.2 °C with an increment of 0.66 °C. Spectra for both the sample and the TPP buffer were collected with the same procedure and the solvent spectra were subtracted from the sample spectra.

Absorptive 2D IR spectra were collected using a 2D IR spectrometer as describe in detail previously.(59) The relative polarizations of the pulses were set to be perpendicular (ZZYY). The waiting time (τ_2) between the first two pulses and the third pulse was fixed at 150 fs. The coherence time between the first and the second pulse was scanned in 4 fs steps from -60 fs to 2.8 ps and 2.0 ps for rephasing and non-rephasing spectra, respectively. The coherence time (τ_1) was Fourier-transformed to obtain the first frequency axis ω_1 . The heterodyned signal was dispersed in a monochromator to obtain the ω_3 frequency dimension and collected using a 64 x 2 pixel mercury-cadmium-telluride (MCT) array detector. Linear absorption from the solvent and solute was divided out along both the ω_1 and ω_3 axes to remove spectral distortions.(60)

Synthesis and purification of double labeled OxyTPP

Details are described in the supplementary material (Supplementary Method M2). Briefly, the 4'-¹⁸O labeled OxyT was synthesized by deamination of thiamine by heating it at 80–90

°C for 12–14 hours in the presence of 10 N sulphuric acid. The 4'-¹⁸O OxyT was double labeled with ³²P or ³³P using thiamine pyrophosphate kinase (TPK). The double labeled OxyTPP was purified first using a 20% denaturing PAGE gel, followed by a 20% native PAGE gel and again with two more rounds of reverse-phase HPLC using C-18 and C-16 columns. The final purified labeled OxyTPP was dissolved in water for binding isotope effects experiments.

Experimental Measurement of Binding Isotope Effects

BIEs were measured for ¹⁸O substitution at the 4'-position of OxyTPP. To monitor OxyTPP substituted with ¹⁸O, it was double labeled with ³³P at terminal phosphate of the pyrophosphate moiety. The OxyTPP with the lighter ¹⁶O isotope was labeled with ³²P. This allowed monitoring of ¹⁸O versus ¹⁶O OxyTPP in the reaction mixture by quantitating ³³P and ³²P radioactivity by scintillation counting. The double labeling scheme provided additional flexibility by switching the labeling pairs, i.e., by combining ¹⁸O with ³²P and ¹⁶O with ³³P. The 4'-¹⁸O BIE was measured as a quotient of the ratio of light to heavy isotope of the bound and free forms of labeled OxyTPP. The riboswitch sequence used in the study is shown in Figure 1B. It was obtained by *in vitro* transcription using T7 Polymerase using double stranded DNA containing the riboswitch sequence and the polymerase binding site cloned into the pUC19 vector (Supplementary Method M3). The [4'-¹⁸O, ³³P] and [4'-¹⁶O, ³³P] double labeled OxyTPPs were synthesized from ¹⁸O and ¹⁶O OxyT using TPK enzyme with ³³P and ³²P ATP labeled at the gamma position, respectively. Reverse pairs were obtained by using ³³P and ³²P labeled ATP with ¹⁶O and ¹⁸O OxyT, respectively, in the TPK reaction.

The protocol used for measuring BIE described elsewhere was modified.⁽⁶¹⁾ BIE reactions were performed in 500 µl reaction volumes containing 100 mM HEPES pH 7.5, 100 mM KCl, 10 mM MgCl₂, 0.1–0.5 µM of OxyTPP and 2.0–5.0 µM of the TPP riboswitch. The ³²P and ³³P labeled OxyTPP were mixed in a 1:3.5 to 1:4.5 ratio for easy deconvolution of the scintillation spectrum to obtain ³²P and ³³P counts. The reaction mixtures were allowed to equilibrate for about 2 hours at 25 °C. The reaction mixtures were applied to Microcon columns with 3000 KDa cutoff filters and centrifuged for about 30 minutes to allow half of the reaction to pass through the filter. Isovolumetric samples (usually about 200 µl) were taken from either side of the filter and transferred into scintillation vials containing 0.8 ml of H₂O and 10 ml Optima Gold scintillation fluid. The contents of the vials were mixed by vigorous shaking. The vials were counted for three cycles of 20 min per sample to obtain ³²P and ³³P counts. The isotope effect was calculated as the quotient of the ratio (light/heavy or ³²P/³³P) of the bound OxyTPP and the ratio of free OxyTPP, quantitated using the following equation:⁽⁶¹⁾

$$BIE = \frac{(((P32/P33) - 1))^{Above}}{(((P32/P33) - 1))^{Below}}$$

The ³²P to ³³P ratio quantitated above and below the filter were used to measure BIEs. The BIEs measured using double labeled OxyTPP contained contributions from both ¹⁸O and ³³P substitutions. It was corrected for the ³³P BIE measured using singly substituted ³³P and ³²P OxyTPPs. To account for the systematic error in the experiment, controls were run using doubly labeled OxyTPP in the absence of the riboswitch. The BIE values were also corrected for ¹⁸O enrichment, measured using a quadrupole time-of-flight (QTOF) mass spectrometer equipped with an electrospray ionization (ESI) source (Supplementary Figure S6), using the following

$$BIE_{corrected} = 1 + \frac{BIE_{observed} - 1}{1 - BIE_{observed}(1 - e)}$$

where e is the isotopic enrichment of the heavy sample. The equation assumes a negligible amount of heavy isotope in the light sample.

Computation of IR spectra and 4'-¹⁸O BIEs for tautomers of OxyT

To help assign the experimental IR spectra, *ab initio* density functional theory (DFT) calculations were performed using QChem.(63) The B3LYP hybrid functional was implemented with the 6-31G (d, p) basis set to optimize the geometry and determine the vibrational normal modes. A harmonic scaling factor of 0.9614 was applied to help match the calculated frequencies with the experiment.(64) The calculations were performed in the gas phase with two explicit D₂O molecules in close proximity of a strong hydrogen bond donor/acceptor such as the carbonyl and amino groups. All labile protons were deuterated to mimic the experimental condition. The same procedure was applied to all three tautomers of oxythiamine: the 4'-keto-N1'H-OxyTPP, 4'-keto-N3'H-OxyTPP, and the 4'-enol-OxyTPP.

The calculations for ¹⁸O BIEs for OxyT were also performed using B3LYP functional and 6-31G (d, p) basis set implemented in Gaussian09.(65) Structures were optimized and the frequencies were calculated using the optimized structures, which were then used to calculate BIEs using ISOEFF98 software(66) at 25 °C using the above mentioned scaling factor.

Solvation effects were examined by the self-consistent reaction field (SCRF) method in Gaussian09. The homogenous dielectric environment was simulated by a virtual solvent characterized by their effective dielectric constants. The calculations were performed in argon, acetonitrile and water, by using the dielectric constants recommended in Gaussian09. The radii used in the SCRF calculations were obtained by running calculations using the volume keyword.

Supplementary Material

Refer to Web version on PubMed Central for supplementary material.

Acknowledgments

This work was supported by NIH Grants CA080024, CA26731, ES002109 and ES007020 to J.M.E.; grants from the NSF (CHE-1212557), the MIT Center for Environmental Health Sciences (NIH Center Grant P30-ES002109), and the MIT Laser Biomedical Research Center (NIH center grant P41-EB015871) to A.T.; NIH traineeship to V.S., and a Poitras Pre-Doctoral Fellowship to C.S.P. We thank Dr. Koli Taghizadeh and Dr. Jeffrey Simpson for help with mass spectrometry and NMR, respectively; Kate MacLean for editorial help; and Sean Karson and Jacqueline Brew for help with T7 Polymerase and TPK enzyme purification, respectively.

References

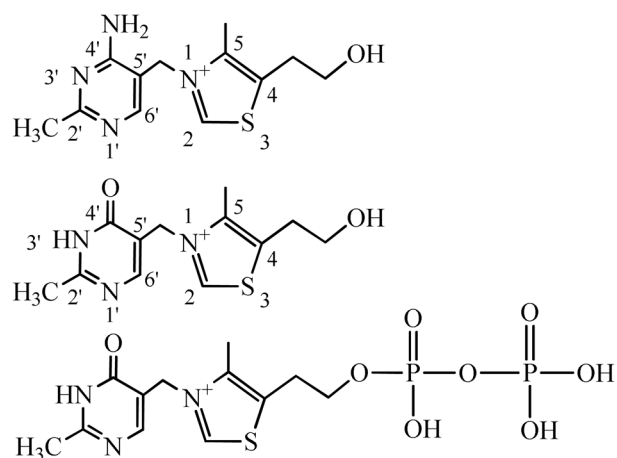
1. Gilbert SD, Reyes FE, Edwards AL, Batey RT. Adaptive ligand binding by the purine riboswitch in the recognition of guanine and adenine analogs. *Structure*. 2009; 17:857–868. [PubMed: 19523903]
2. Cochrane JC, Strobel SA. Catalytic Strategies of Self-Cleaving Ribozymes. *Acc Chem Res*. 2008; 41:1027–1035. [PubMed: 18652494]
3. Cochrane JC, Lipchock SV, Strobel SA. Structural Investigation of the GlmS Ribozyme Bound to Its Catalytic Cofactor. *Chemistry & Biology*. 2007; 14:97–105. [PubMed: 17196404]

4. Wilson TJ, Ouellet J, Zhao Z-Y, Harusawa S, Araki L, Kurihara T, Lilley DMJ. Nucleobase catalysis in the hairpin ribozyme. *RNA*. 2006; 12:980–987. [PubMed: 16601203]
5. Han J, Burke JM. Model for general acid-base catalysis by the hammerhead ribozyme: pH-activity relationships of G8 and G12 variants at the putative active site. *Biochemistry*. 2005; 44:7864–7870. [PubMed: 15910000]
6. Goodman MF. Mutations caught in the act. *Nature*. 1995; 378:237–238. [PubMed: 7477337]
7. Lippert B, Gupta D. Promotion of rare nucleobase tautomers by metal binding. *Dalton Transactions*. 2009:4619. [PubMed: 19513468]
8. Löwdin PO. Proton Tunneling in DNA and its Biological Implications. *Rev Mod Phys*. 1963; 35:724–732.
9. Miles HT. Tautomeric Forms in a Polynucleotide Helix and Their Bearing on the Structure of Dna. *PNAS*. 1961; 47:791–802. [PubMed: 13770642]
10. Pérez A, Tuckerman ME, Hjalmarson HP, von Lilienfeld OA. Enol Tautomers of Watson-Crick Base Pair Models Are Metastable Because of Nuclear Quantum Effects. *J Am Chem Soc*. 2010; 132:11510–11515. [PubMed: 20681591]
11. Stolarski R, Kierdaszuk B, Hagberg CE, Shugar D. Mechanism of hydroxylamine mutagenesis: tautomeric shifts and proton exchange between the promutagen N6-methoxyadenosine and cytidine. *Biochemistry*. 1987; 26:4332–4337. [PubMed: 3663593]
12. Strazewski P. Mismatch formation in DNA can involve rare tautomeric forms in the template. *Nucl Acids Res*. 1988; 16:9377–9398. [PubMed: 3054806]
13. Wang W, Hellinga HW, Beese LS. Structural evidence for the rare tautomer hypothesis of spontaneous mutagenesis. *PNAS*. 2011; 108:17644–17648. [PubMed: 22006298]
14. Thore S, Frick C, Ban N. Structural Basis of Thiamine Pyrophosphate Analogues Binding to the Eukaryotic Riboswitch. *J Am Chem Soc*. 2008; 130:8116–8117. [PubMed: 18533652]
15. Wilcox JL, Ahluwalia AK, Bevilacqua PC. Charged Nucleobases and Their Potential for RNA Catalysis. *Acc Chem Res*. 2011; 44:1270–1279. [PubMed: 21732619]
16. Bevilacqua PC, Brown TS, Nakano S, Yajima R. Catalytic roles for proton transfer and protonation in ribozymes. *Biopolymers*. 2004; 73:90–109. [PubMed: 14691943]
17. Gong B, Klein DJ, Ferré-D'Amaré AR, Carey PR. The glmS Ribozyme Tunes the Catalytically Critical pKa of Its Coenzyme Glucosamine-6-phosphate. *J Am Chem Soc*. 2011; 133:14188–14191. [PubMed: 21848325]
18. Lupták A, Ferré-D'Amaré AR, Zhou K, Zilm KW, Doudna JA. Direct pK(a) measurement of the active-site cytosine in a genomic hepatitis delta virus ribozyme. *J Am Chem Soc*. 2001; 123:8447–8452. [PubMed: 11525650]
19. Liu L, Cottrell JW, Scott LG, Fedor MJ. Direct measurement of the ionization state of an essential guanine in the hairpin ribozyme. *Nat Chem Biol*. 2009; 5:351–357. [PubMed: 19330013]
20. Chatake T, Ono A, Ueno Y, Matsuda A, Takénaka A. Crystallographic studies on damaged DNAs. I An N(6)-methoxyadenine residue forms a Watson-Crick pair with a cytosine residue in a B-DNA duplex. *J Mol Biol*. 1999; 294:1215–1222. [PubMed: 10600379]
21. Watson JD, Crick FHC. Molecular Structure of Nucleic Acids: A Structure for Deoxyribose Nucleic Acid. *Nature*. 1953; 171:737–738. [PubMed: 13054692]
22. Watson JD, Crick FHC. Genetical Implications of the Structure of Deoxyribonucleic Acid. *Nature*. 1953; 171:964–967. [PubMed: 13063483]
23. Hunter WN, Brown T, Anand NN, Kennard O. Structure of an adenine-cytosine base pair in DNA and its implications for mismatch repair. *Nature*. 1986; 320:552–555. [PubMed: 3960137]
24. Beak P. Energies and alkylations of tautomeric heterocyclic compounds: old problems - new answers. *Acc Chem Res*. 1977; 10:186–192.
25. Fujimoto A, Inuzuka K, Shiba R. Electronic Properties and p- p* Absorption Spectrum of 2-Pyridone. *Bull Chem Soc Jpn*. 1981; 54:2802–2806.
26. Katritzky AR, Popp FD, Rowe JD. Potentially tautomeric pyridines. Part VII. Glutaconimide and its methyl derivatives. *J Chem Soc B*. 1966:562–564.
27. Kühne R, Schaffhauser T, Wokaun A, Ernst R. Study of transient chemical reactions by NMR. Fast stopped-flow fourier transform experiments. *J Magn Reson* (1969). 1979; 35:39–67.

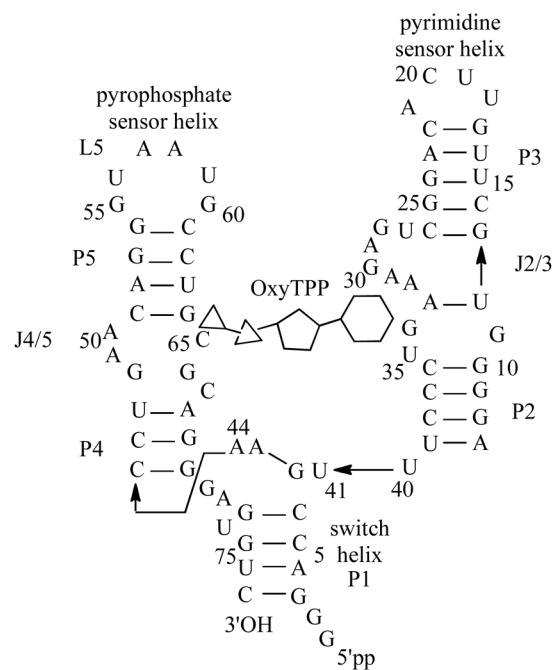
28. Jaworski A, Szczesniak M, Szczepaniak K, Kubulat K, Person WB. Infrared spectra and tautomerism of 5-fluorocytosine, 5-bromocytosine and 5-iodocytosine. Matrix isolation and theoretical AB initio studies. *J Mol Struct.* 1990; 223:63–92.
29. Mons M, Dimicoli I, Piuzzi F, Tardivel B, Elhanine M. Tautomerism of the DNA Base Guanine and Its Methylated Derivatives as Studied by Gas-Phase Infrared and Ultraviolet Spectroscopy. *J Phys Chem A.* 2002; 106:5088–5094.
30. Bakker JM, Compagnon I, Meijer G, von Helden G, Kabeláb M, Hobza P, de Vries MS. The mid-IR absorption spectrum of gas-phase clusters of the nucleobases guanine and cytosine. *Phys Chem Chem Phys.* 2004; 6:2810–2815.
31. Viladoms J, Scott LG, Fedor MJ. An active-site guanine participates in glmS ribozyme catalysis in its protonated state. *J Am Chem Soc.* 2011; 133:18388–18396. [PubMed: 21936556]
32. Wilcox JL, Bevilacqua PC. A simple fluorescence method for pK(a) determination in RNA and DNA reveals highly shifted pK(a)'s. *J Am Chem Soc.* 2013; 135:7390–7393. [PubMed: 23432144]
33. Guo M, Spitale RC, Volpini R, Krucinska J, Cristalli G, Carey PR, Wedekind JE. Direct Raman measurement of an elevated base pKa in the active site of a small ribozyme in a precatalytic conformation. *J Am Chem Soc.* 2009; 131:12908–12909. [PubMed: 19702306]
34. Gong B, Chen J-H, Yajima R, Chen Y, Chase E, Chadalavada DM, Golden BL, Carey PR, Bevilacqua PC. Raman crystallography of RNA. *Methods.* 2009; 49:101–111. [PubMed: 19409996]
35. Peng CS, Tokmakoff A. Identification of Lactam–Lactim Tautomers of Aromatic Heterocycles in Aqueous Solution Using 2D IR Spectroscopy. *J Phys Chem Lett.* 2012; 3:3302–3306. [PubMed: 23227298]
36. Peng CS, Baiz CR, Tokmakoff A. Direct observation of ground-state lactam–lactim tautomerization using temperature-jump transient 2D IR spectroscopy. *PNAS.* 2013; 110:9243–9248. [PubMed: 23690588]
37. Natalya V, Belova HO. The keto/enol tautomerism in acetoacetyl fluoride: properties, spectroscopy, and gas-phase and crystal structures of the enol form. *Phys Chem Chem Phys.* 2010; 12:11445–53. [PubMed: 20683513]
38. Hamm, P.; Zanni, M. *Concepts and Methods of 2D Infrared Spectroscopy.* 1. Cambridge University Press; 2011.
39. Messmer AT, Lippert KM, Schreiner PR, Bredenbeck J. Structure analysis of substrate catalyst complexes in mixtures with ultrafast two-dimensional infrared spectroscopy. *Phys Chem Chem Phys.* 2013; 15:1509–1517. [PubMed: 23238288]
40. Peng CS, Jones KC, Tokmakoff A. Anharmonic Vibrational Modes of Nucleic Acid Bases Revealed by 2D IR Spectroscopy. *J Am Chem Soc.* 2011; 133:15650–15660. [PubMed: 21861514]
41. Sung J, Silbey RJ. Four wave mixing spectroscopy for a multilevel system. *J Chem Phys.* 2001; 115:9266–9287.
42. Schramm VL. Binding isotope effects: boon and bane. *Curr Opin Chem Biol.* 2007; 11:529–536. [PubMed: 17869163]
43. Gawlita E, Paneth P, Anderson VE. Equilibrium isotope effect on ternary complex formation of [1-18O]oxamate with NADH and lactate dehydrogenase. *Biochemistry.* 1995; 34:6050–6058. [PubMed: 7742308]
44. Andersson L, MacNeela J, Wolfenden R. Use of secondary isotope effects and varying pH to investigate the mode of binding of inhibitory amino aldehydes by leucine aminopeptidase. *Biochemistry.* 1985; 24:330–333. [PubMed: 3978076]
45. Bush K, Mahler HR, Shiner VJ Jr. Deuterium effects on binding of reduced coenzyme alcohol dehydrogenase isoenzyme EE. *Science.* 1971; 172:478–480. [PubMed: 4323799]
46. Lewis BE, Schramm VL. Binding equilibrium isotope effects for glucose at the catalytic domain of human brain hexokinase. *J Am Chem Soc.* 2003; 125:4785–4798. [PubMed: 12696897]
47. Taylor, JR. *An Introduction to Error Analysis: The Study of Uncertainties in Physical Measurements.* University Science Books; 1997.

48. Thore S, Leibundgut M, Ban N. Structure of the Eukaryotic Thiamine Pyrophosphate Riboswitch with Its Regulatory Ligand. *Science*. 2006; 312:1208–1211. [PubMed: 16675665]
49. Winkler W, Nahvi A, Breaker RR. Thiamine derivatives bind messenger RNAs directly to regulate bacterial gene expression. *Nature*. 2002; 419:952–956. [PubMed: 12410317]
50. Sudarsan N, Barrick JE, Breaker RR. Metabolite-binding RNA domains are present in the genes of eukaryotes. *RNA*. 2003; 9:644–647. [PubMed: 12756322]
51. Thore S, Leibundgut M, Ban N. Structure of the Eukaryotic Thiamine Pyrophosphate Riboswitch with Its Regulatory Ligand. *Science*. 2006; 312:1208–1211. [PubMed: 16675665]
52. Yamauchi T, Miyoshi D, Kubodera T, Nishimura A, Nakai S, Sugimoto N. Roles of Mg²⁺ in TPP-dependent riboswitch. *FEBS Letters*. 2005; 579:2583–2588. [PubMed: 15862294]
53. Kulshina N, Edwards TE, Ferré-D'Amaré AR. Thermodynamic analysis of ligand binding and ligand binding-induced tertiary structure formation by the thiamine pyrophosphate riboswitch. *RNA*. 2010; 16:186–196. [PubMed: 19948769]
54. Dedon PC, Tannenbaum SR. Reactive nitrogen species in the chemical biology of inflammation. *Arch Biochem Biophys*. 2004; 423:12–22. [PubMed: 14989259]
55. Gangolf M, Czerniecki J, Radermecker M, Detry O, Nisolle M, Jouan C, Martin D, Chantraine F, Lakaye B, Wins P, Grisar T, Bettendorff L. Thiamine Status in Humans and Content of Phosphorylated Thiamine Derivatives in Biopsies and Cultured Cells. *PLoS ONE*. 2010; 5:e13616. [PubMed: 21049048]
56. Serganov A, Polonskaia A, Phan AT, Breaker RR, Patel DJ. Structural basis for gene regulation by a thiamine pyrophosphate-sensing riboswitch. *Nature*. 2006; 441:1167–1171. [PubMed: 16728979]
57. Harris KS, Brabant W, Styrchak S, Gall A, Daifuku R. KP-1212/1461, a nucleoside designed for the treatment of HIV by viral mutagenesis. *Antiviral Res*. 2005; 67:1–9. [PubMed: 15890415]
58. Fox EJ, Loeb LA. Lethal Mutagenesis: targeting the mutator phenotype in cancer. *Semin Cancer Biol*. 2010; 20:353–359. [PubMed: 20934515]
59. Chung HS, Khalil M, Smith AW, Tokmakoff A. Transient two-dimensional IR spectrometer for probing nanosecond temperature-jump kinetics. *Rev Sci Instrum*. 2007; 78:063101. [PubMed: 17614599]
60. Jones KC, Ganim Z, Peng CS, Tokmakoff A. Transient two-dimensional spectroscopy with linear absorption corrections applied to temperature-jump two-dimensional infrared. *J Opt Soc Am B*. 2012; 29:118–129.
61. Murkin AS, Birck MR, Rinaldo-Matthis A, Shi W, Taylor EA, Almo SC, Schramm VL. Neighboring group participation in the transition state of human purine nucleoside phosphorylase. *Biochemistry*. 2007; 46:5038–5049. [PubMed: 17407325]
62. Caldwell SR, Raushel FM, Weiss PM, Cleland WW. Transition-state structures for enzymatic and alkaline phosphotriester hydrolysis. *Biochemistry*. 1991; 30:7444–7450. [PubMed: 1649629]
63. Shao Y, et al. Advances in methods and algorithms in a modern quantum chemistry program package. *Phys Chem Chem Phys*. 2006; 8:3172–3191. [PubMed: 16902710]
64. Scott AP, Radom L. Harmonic Vibrational Frequencies:3 An Evaluation of Hartree-Fock, Møller-Plesset, Quadratic Configuration Interaction, Density Functional Theory, and Semiempirical Scale Factors. *J Phys Chem*. 1996; 100:16502–16513.
65. Frisch, M., et al. Gaussian09. Gaussian Inc; Wallingford CT: 2009.
66. Anisimov V, Paneth P. ISOEFF98. A program for studies of isotope effects using Hessian modifications. *J Math Chem*. 1999; 26:75–86.

A.



B.

**Figure 1.**

A. Structures of thiamine (T) (top), oxythiamine (OxyT) (middle) and oxythiamine pyrophosphate (OxyTPP) (bottom) **B.** Secondary structure and sequence of the TPP riboswitch from *Arabidopsis thaliana* (adapted from reference (48)) used in the study.

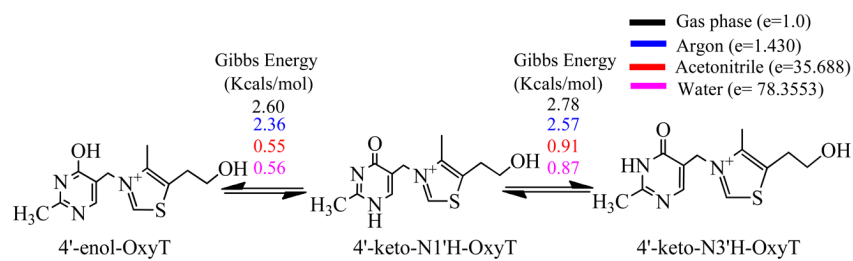


Figure 2. Tautomers of OxyT and their relative Gibbs energies calculated in Gaussian09 using B3LYP functional and 6-31G (d, p) basis set in the presence of explicit water molecules and various implicit environments (vacuum, argon, acetonitrile and water).

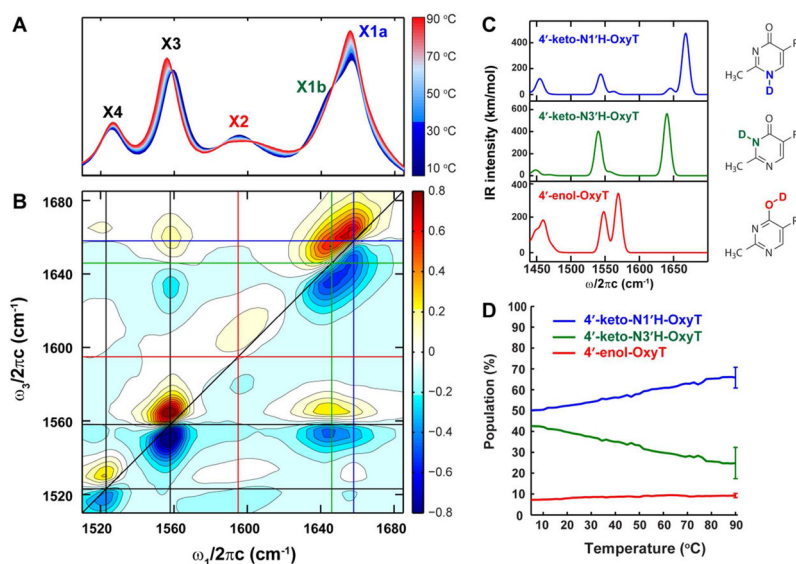


Figure 3.

A. FTIR spectra of OxyT in TPP buffer taken at various temperatures (5 °C – 90 °C); **B.** 2D IR spectrum of OxyT under the same solvent condition at 10 °C; **C.** DFT calculated IR spectra for the three OxyT tautomers using QChem. The frequencies have been scaled by 0.9614; **D.** Temperature dependence of populations of tautomers of OxyT. The populations were obtained from fitting the variable temperature FTIR spectra (Figure S6). Representative error bars are shown at 90 °C and are roughly independent of temperature.

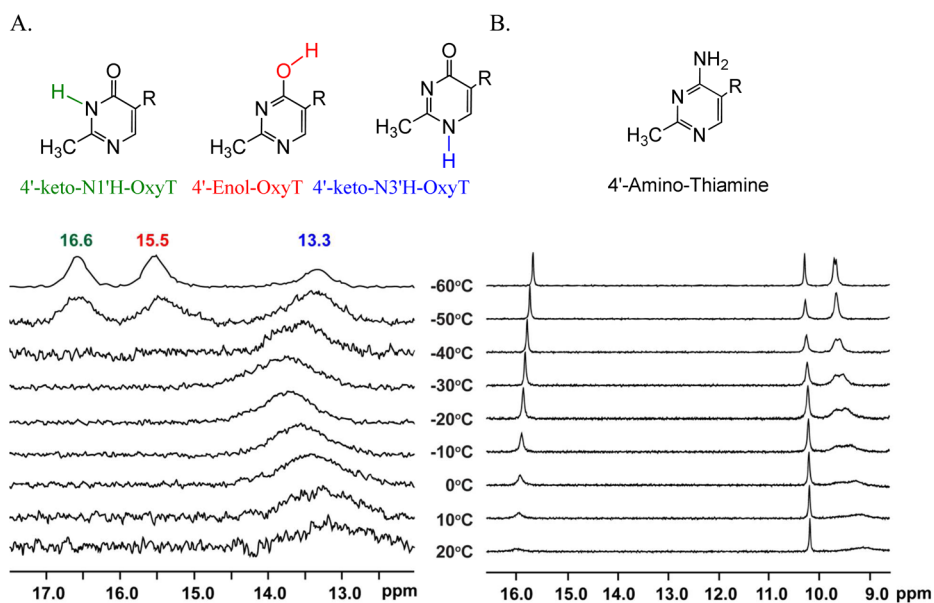
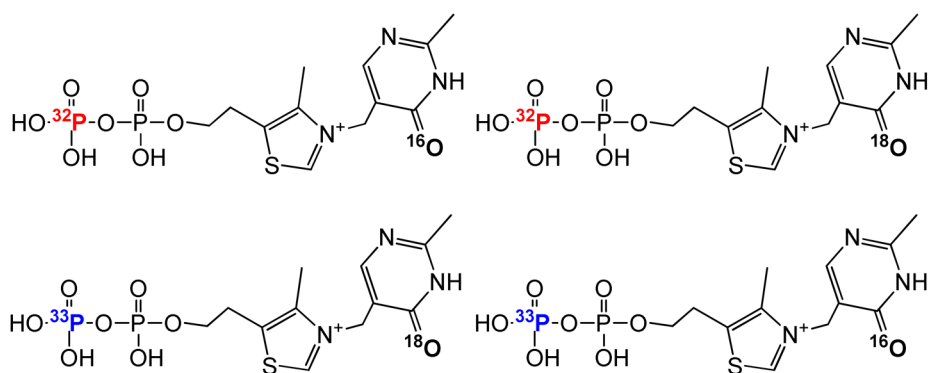


Figure 4.
A. Variable temperature ^1H NMR spectra of oxythiamine in DMF-d_7 (20 °C to -60 °C); **B.** Variable temperature ^1H NMR spectra of thiamine in DMF-d_7 (20 °C to -60 °C). The thiamine spectra were assigned according to SDBS database (Supplementary material; Note 3).



Labeling Scheme and 4'- ^{18}O BIE

$[(^{32}\text{P}, ^{16}\text{O}) \text{ and } (^{33}\text{P}, ^{18}\text{O})]$ OxyTPP

$$4'\text{-}^{18}\text{O BIE} = 0.982 \pm 0.004$$

Labeling Scheme and 4'- ^{18}O BIE

$[(^{32}\text{P}, ^{18}\text{O}) \text{ and } (^{33}\text{P}, ^{16}\text{O})]$ OxyTPP

$$4'\text{-}^{18}\text{O BIE} = 0.985 \pm 0.004$$

Figure 5.

Structures of OxyTPP showing the numbering and the labeling schemes for different isotopes used for measuring BIEs and the values of 4'- ^{18}O BIEs measured using double labeled OxyTPP and the TPP riboswitch (as shown in Figure 1B).

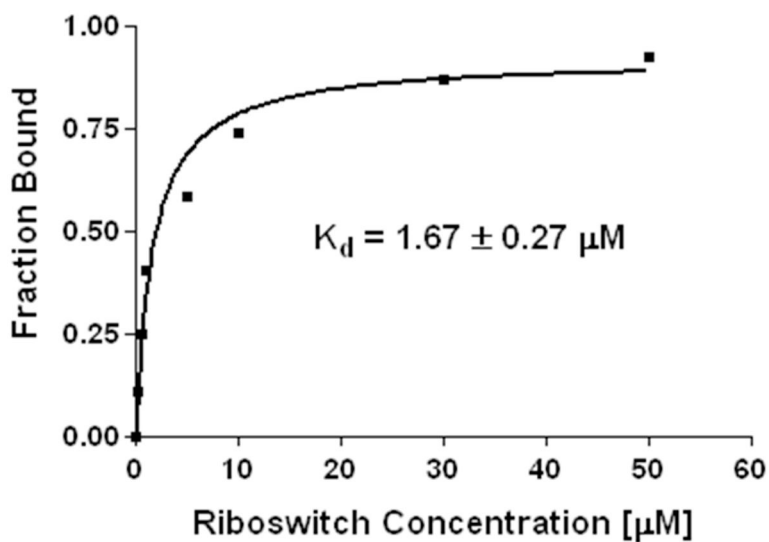


Figure 6. Binding of the TPP riboswitch to ^{33}P labeled OxyTPP. The K_d value was measured after 2 hr incubation of binding reactions containing TPP buffer (methods section), 100 nM ^{33}P labeled OxyTPP and various concentrations of the TPP riboswitch (0.1, 0.5, 1, 5, 10, 30, 50 μM).

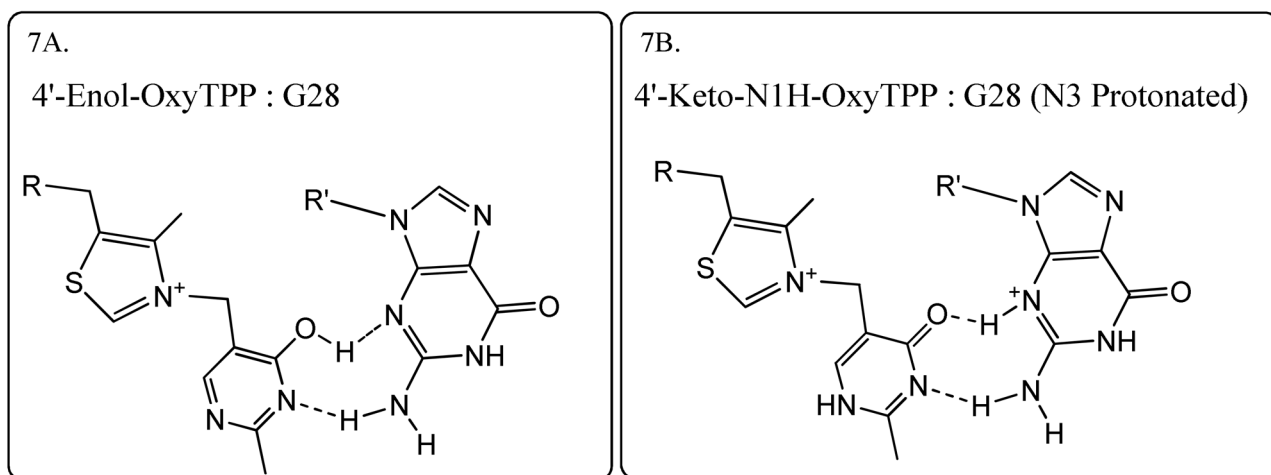
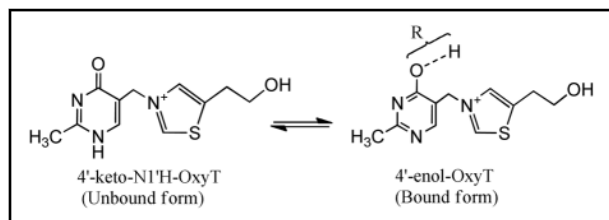


Figure 7. Proposed models showing interactions for both enol and keto tautomers of OxyTPP (4'-Enol-OxyTPP and 4'-keto-N1H-OxyTPP) with the G28 of the TPP riboswitch, that are consistent with the crystal structure of the riboswitch with OxyTPP.(14)

Table 1

The $4\text{-}^{18}\text{O}$ BIEs due to polarization of the $4'$ -hydroxyl group of $4'$ -enol-OxyT. BIEs are calculated relative to $4'$ -keto-N $1'$ H-OxyT, as shown on the top. BIEs were calculated using ISOEFF98 from frequencies obtained by using the B3LYP functional and 6-31G (d, p) basis set implemented in Gaussian 09.



4'-OH bond length in angstroms (Å)	[4- ^{18}O] BIE
0.971 Å	1.001
1.0 Å	1.001
1.1 Å	1.006
1.2 Å	1.013
1.3 Å	1.022
1.4 Å	1.023
1.5 Å	1.025
1.6 Å	1.028
1.7 Å	1.030
1.8 Å	1.030
1.9 Å	1.032
2.0 Å	1.032

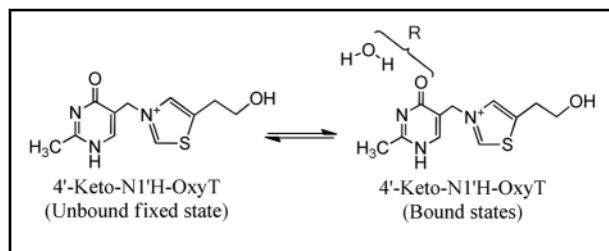
Table 2

The calculated 4'-¹⁸O BIEs from interconversion of tautomers of OxyT. BIEs were calculated using ISOEFF98 and Gaussian09.

Interconversion of Tautomers	4'- ¹⁸ O BIEs
4'-keto-N3'H-OxyT to 4'-keto-N1'H-OxyT	0.998
4'-enol-OxyT to 4'-keto-N3'H-OxyT	0.999
4'-enol-OxyT to 4'-keto-N1'H-OxyT	1.002

Table 3

The calculated 4'-¹⁸O BIEs due to hydrogen bonding to the 4'-keto-N1'H-OxyT tautomer. BIEs were calculated relative to the 4'-keto-N1'H-OxyT, as shown on the top, using ISOEFF98 and Gaussian09.



O ^{Wat} -O ^{OxyT} Distance (R)	[4'- ¹⁸ O] BIEs
2.00 Å	0.9714
2.10 Å	0.9788
2.12 Å	0.9801
2.14 Å	0.9813
2.16 Å	0.9824
2.18 Å	0.9835
2.20 Å	0.9844
2.22 Å	0.9854
2.24 Å	0.9863
2.26 Å	0.9871
2.28 Å	0.9880
2.30 Å	0.9917
2.40 Å	0.9931
2.50 Å	0.9934
2.60 Å	0.9939
2.70 Å	0.9951
2.80 Å	0.9959
2.90 Å	0.9966
3.00 Å	0.9971